# Thermal freeze-out versus chemical freeze-out revised

Dariusz Prorok
*Institute of Theoretical Physics, University of Wrocław,*
*Pl.Maksa Borna 9, 50-204 Wrocław, Poland*
(Dated: February 12, 2007)

A competitive, to the commonly used blast-wave, model describing the freeze-out hypersurface is applied to fit the $p_T$-spectra of identified hadrons measured at relativistic heavy-ion collisions at $\sqrt{s_{NN}} = 62.4,\ 130$ and 200 GeV. Decays of resonances are taken into account completely. It has turned out that the fitted kinetic freeze-out temperature and baryon number chemical potential depend weakly on the centrality of the collision and their values are close to the chemical freeze-out values determined from fits to particle yield ratios.

PACS numbers: 25.75.-q, 25.75.Dw, 24.10.Pa, 24.10.Jv

During a heavy-ion collision a hot and dense medium is created which eventually evolves into a state of freely streaming particles. The process of hadron decoupling is called *freeze-out* and two kinds of freeze-out are distinguished [1, 2]: (i) *chemical freeze-out* at $T_{chem}$ when the hadron abundances become fixed and (ii) *thermal (kinetic) freeze-out* at $T_{kin}$ when elastic rescattering processes cease and hadrons start to escape freely. And $T_{chem} \geq T_{kin}$ is expected. Values of the statistical parameters at the chemical freeze-out are determined from fits to particle yield ratios, whereas corresponding values at the kinetic freeze-out are fitted to the spectra of hadrons. $T_{chem} \sim 150 - 170$ MeV is estimated at highest heavy-ion reaction energy [3, 4, 5, 6, 7, 8, 9, 10, 11, 12, 13]. Additionally, fits done for various centrality classes have revealed that $T_{chem}$ is almost independent of centrality [4, 6, 8, 9, 10]. On the contrary, the temperature at the kinetic freeze-out depends on the centrality and is substantially lower. From the most central to the peripheral bin it changes as follows: $T_{kin} = 121 - 161$ MeV for PHENIX at $\sqrt{s_{NN}} = 130$ GeV [14], $T_{kin} = 111 - 147$ MeV for PHENIX at $\sqrt{s_{NN}} = 200$ GeV [15], $T_{kin} = 89 - 129$ MeV for STAR at $\sqrt{s_{NN}} = 200$ GeV [9] and $T_{kin} = 110 - 115$ MeV for BRAHMS at $\sqrt{s_{NN}} = 200$ GeV [16]. For the PHOBOS data at $\sqrt{s_{NN}} = 62.4$ GeV $T_{kin} = 103, 102, 101$ MeV for the central, mid-peripheral and peripheral bin, respectively [17]. However, the aforementioned estimates of $T_{kin}$ have been done within the very simplified hydrodynamic model, *i.e.* the blast-wave model [18].

In this Letter, we will show that the behavior of $T_{kin}$ is model dependent and within a different hypersurface and with complete treatment of resonance decays different conclusions about statistical parameters at the kinetic freeze-out can be obtained. Namely, the statistical parameters at the kinetic freeze-out are roughly centrality independent and their values are close to the corresponding values at the chemical freeze-out.

The model applied here is inspired by the single-freeze-out model of Refs. [19, 20], but its crucial assumption about one freeze-out *is dismissed*. The foundations of the model are as follows: $(a)$ a freeze-out hypersurface is defined by the equation $\tau = \sqrt{t^2 - r_x^2 - r_y^2 - r_z^2} = const$, $(b)$ the four-velocity of an element of the freeze-out hypersurface is proportional to its coordinate, $u^\mu = x^\mu/\tau$, $(c)$ the transverse size is restricted by the condition $r = \sqrt{r_x^2 + r_y^2} < \rho_{max}$, $(d)$ all confirmed resonances up to a mass of 2 GeV from the Particle Data Tables [21] are taken into account, $(e)$ primordial distributions of the constituents of the gas at the kinetic freeze-out are Bose-Einstein or Fermi-Dirac, $(f)$ resonance decays (including weak decays) are incorporated, $(g)$ the following parameterization of the hypersurface is chosen

$$t = \tau \cosh\alpha_\parallel \cosh\alpha_\perp, \quad r_x = \tau \sinh\alpha_\perp \cos\phi,$$
$$r_y = \tau \sinh\alpha_\perp \sin\phi, \quad r_z = \tau \sinh\alpha_\parallel \cosh\alpha_\perp. \qquad (1)$$

The model has four parameters, the two thermal parameters, the temperature $T_{kin}$ and the baryon number chemical potential $\mu_B$, and the two geometric parameters, $\tau$ and $\rho_{max}$. The maximum transverse-flow parameter is expressed as $\beta_\perp^{max} = (\rho_{max}/\tau)/(\sqrt{1 + (\rho_{max}/\tau)^2})$. The invariant distribution of the measured particles of species $i$ has the form [19, 20]

$$\frac{dN_i}{d^2p_T\, dy} = \tau^3 \int_{-\infty}^{+\infty} d\alpha_\parallel \int_0^{\rho_{max}/\tau} \sinh\alpha_\perp d(\sinh\alpha_\perp) \times \int_0^{2\pi} d\xi\ (p\cdot u)\ f_i(p\cdot u)\ , \qquad (2)$$

where $p \cdot u = m_T \cosh(\alpha_\parallel - y) \cosh\alpha_\perp - p_T \cos\xi \sinh\alpha_\perp$ and $f_i$ is the final momentum distribution of the particle in question, what means that $f_i$ is the sum of primordial and simple and sequential decay contributions to the particle distribution (for details of the treatment of decays see Ref. [22]). With the use of Eq. (2) the measured transverse-momentum spectra of $\pi^\pm$, $K^\pm$, $p$ and $\bar{p}$ [9, 14, 16, 17, 23] can be fitted to determine values of the parameters of the model (data points with $p_T > 3$ GeV have been excluded). Fits are performed with the help of

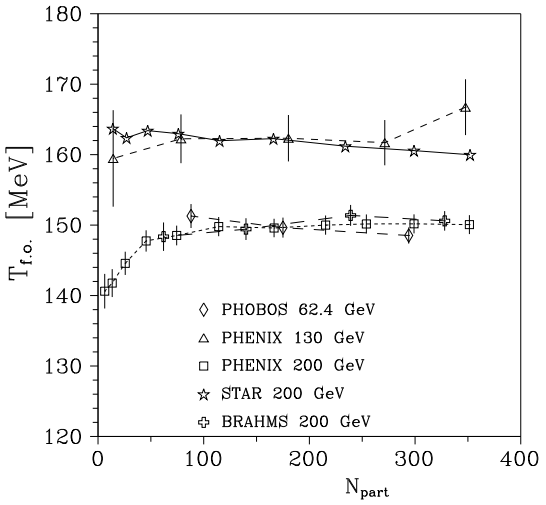


FIG. 1: Centrality dependence of the kinetic freeze-out temperature for the RHIC measurements at $\sqrt{s_{NN}} = 62.4,\ 130$ and 200 GeV. The lines connect the results and are a guide.

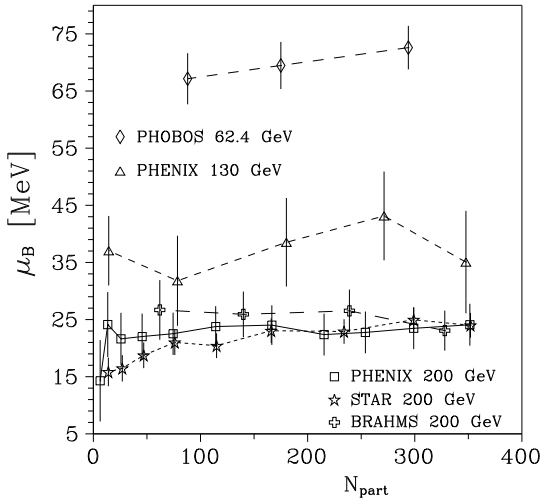


FIG. 2: Centrality dependence of the baryon number chemical potential for the RHIC measurements at $\sqrt{s_{NN}} = 62.4,\ 130$ and 200 GeV. The lines connect the results and are a guide.

the $\chi^2$ method. It should be stressed that now all four parameters of the model ($T_{kin}$, $\mu_B$, $\rho_{max}$ and $\tau$) are fitted simultaneously, opposite to the case of Refs. [19, 20] where the determination proceeded in two steps. First, statistical parameters $T$ and $\mu_B$ were fitted with the use of the experimental ratios of hadron multiplicities at midrapidity. Then geometric parameters were determined from fits to the transverse-momentum spectra. Therefore the assumption that the chemical freeze-out happens simultaneously with the kinetic freeze-out (the single freeze-out) was crucial in that approach. Now all parameters are fitted to the spectra, so the aforementioned assumption is omitted and values of statistical parameters have the meaning of the values at the kinetic freeze-out.

The fitted results for $T_{kin}$, $\mu_B$, $\rho_{max}$ and $\tau$ are gathered in Table I together with values of the surface velocity $\beta_\perp^{max}$ and values of $\chi^2$/NDF for each centrality class additionally characterized by the number of participants $N_{part}$. Note that except the most peripheral bins of the PHENIX measurements all fits are statistically significant. Results for $T_{kin}$ and $\mu_B$ are also depicted as functions of $N_{part}$ in Figs. 1 and 2, respectively. It is clearly seen that both $T_{kin}$ and $\mu_B$ are almost independent of the collision centrality, only for peripheral bins some dependence can be observed. Additionally, their values are very close to the values at the chemical freeze-out. Namely, $T_{chem} = 165 - 169$ MeV and $\mu_B = 33 - 38$ MeV from the peripheral to most central bin at $\sqrt{s_{NN}} = 130$ GeV was found in Ref. [6], $T_{chem} \approx 155$ MeV and $\mu_B \approx 26$ MeV independent of the centrality for PHENIX at $\sqrt{s_{NN}} = 200$ GeV in Ref. [8] and $T_{chem} \approx 160$ MeV independent of the centrality and $\mu_B = 15 - 24$ MeV from the peripheral to most central bin for STAR at $\sqrt{s_{NN}} = 200$ GeV in Refs. [9, 10, 11].

As a simple test of the self-consistency of the model the total charged-particle multiplicity, $N_{ch}$, has been estimated with the use of the fitted parameters from Table I. The reasons for choosing $N_{ch}$ are as follows: it is measured independently of hadron spectroscopy and in the whole rapidity range [24] and is given by a simple formula in the model. Namely, $N_{ch} = 2\pi\ \alpha_\parallel^{max} \tau \rho_{max}^2\ n_{ch}(T, \mu_B)$, where $n_{ch}(T, \mu_B)$ is the final charged particle density for a static gas and $\alpha_\parallel^{max}(c) = y_p - \frac{\langle \delta y \rangle}{0.975} \cdot (1 - c)$ is the maximal value of the rapidity of the fluid element, $y_p$ is the projectile rapidity, $\langle \delta y \rangle$ the average rapidity loss and $c$ is a fractional number representing the middle of a given centrality bin, i.e. $c = 0.025$ for the $0 - 5\%$ centrality bin, etc. (for details see Ref. [25]). The BRAHMS Col-

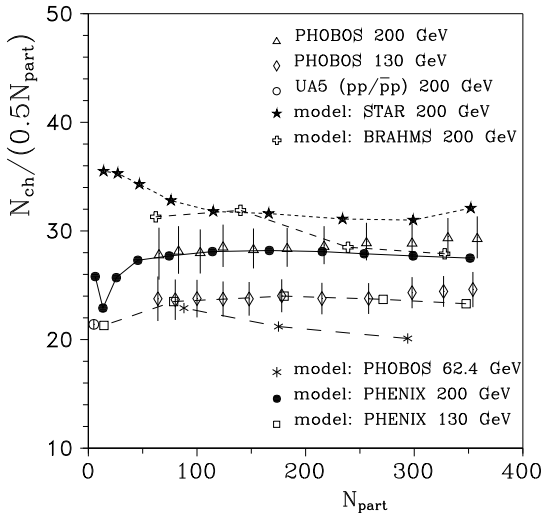


FIG. 3: $N_{ch}$ per pair of participants versus $N_{part}$ for RHIC at $\sqrt{s_{NN}} = 62.4,\ 130$ and 200 GeV. The PHOBOS data are from [24] and the $pp/\bar{p}p$ data point of the UA5 measurement is from Fig.39.5 in [21]. The lines connect the results and are a guide.

TABLE I: Values of the statistical and geometric parameters of the model for various centrality bins fitted with the use of the RHIC final data for the $p_T$ spectra of identified charged hadrons [9, 14, 16, 23]. All data are at midrapidity, except the PHOBOS case (first three rows) where data are at $y = 0.8$ [17].

| Au-Au collision case | Centrality [%] | $N_{part}$ | $T_{kin}$ [MeV] | $\mu_B$ [MeV] | $\rho_{max}$ [fm] | $\tau$ [fm] | $\beta_\perp^{max}$ | $\chi^2$/NDF | NDF |
|---|---|---|---|---|---|---|---|---|---|
| PHOBOS at | 0-15 | 294.0 | 148.52±1.15 | 72.60±3.81 | 7.84±0.19 | 8.35±0.14 | 0.68 | 0.995 | 72 |
| $\sqrt{s_{NN}} = 62.4$ GeV | 15-30 | 175.0 | 149.64±1.42 | 69.47±4.13 | 6.23±0.19 | 7.20±0.17 | 0.65 | 0.43 | 72 |
| | 30-50 | 88.0 | 151.29±1.70 | 67.15±4.47 | 4.60±0.18 | 6.05±0.18 | 0.61 | 0.20 | 71 |
| | 0-5 | 347.7 | 166.74±3.96 | 35.06±8.97 | 6.31±0.41 | 8.08±0.44 | 0.62 | 0.53 | 78 |
| PHENIX at | 5-15 | 271.3 | 161.70±3.21 | 43.14±7.77 | 6.34±0.35 | 7.57±0.34 | 0.64 | 0.46 | 78 |
| $\sqrt{s_{NN}} = 130$ GeV | 15-30 | 180.2 | 162.33±3.29 | 38.52±7.75 | 5.32±0.29 | 6.54±0.29 | 0.63 | 0.50 | 78 |
| | 30-60 | 78.5 | 162.25±3.46 | 31.80±7.87 | 3.77±0.23 | 4.95±0.23 | 0.61 | 0.75 | 78 |
| | 60-92 | 14.3 | 159.46±6.85 | 37.05±16.09 | 1.87±0.27 | 3.26±0.27 | 0.50 | 1.37 | 42 |
| | 0-5 | 351.4 | 150.07±1.34 | 24.10±3.66 | 9.28±0.21 | 9.48±0.19 | 0.70 | 0.69 | 122 |
| PHENIX at | 5-10 | 299.0 | 150.18±1.35 | 23.48±3.65 | 8.75±0.20 | 8.80±0.18 | 0.70 | 0.50 | 122 |
| $\sqrt{s_{NN}} = 200$ GeV | 10-15 | 253.9 | 150.16±1.35 | 22.75±3.65 | 8.25±0.19 | 8.20±0.17 | 0.71 | 0.37 | 122 |
| | 15-20 | 215.3 | 150.00±1.36 | 22.38±3.65 | 7.80±0.18 | 7.69±0.16 | 0.71 | 0.37 | 122 |
| | 20-30 | 166.6 | 149.59±1.31 | 24.03±3.47 | 7.13±0.16 | 6.96±0.14 | 0.72 | 0.45 | 122 |
| | 30-40 | 114.2 | 149.79±1.36 | 23.78±3.56 | 6.14±0.14 | 6.03±0.12 | 0.71 | 0.66 | 122 |
| | 40-50 | 74.4 | 148.53±1.40 | 22.52±3.71 | 5.28±0.13 | 5.27±0.11 | 0.71 | 0.89 | 122 |
| | 50-60 | 45.5 | 147.75±1.51 | 22.02±4.03 | 4.38±0.12 | 4.55±0.10 | 0.69 | 0.96 | 122 |
| | 60-70 | 25.7 | 144.57±1.65 | 21.63±4.56 | 3.63±0.11 | 3.91±0.09 | 0.68 | 1.12 | 122 |
| | 70-80 | 13.4 | 141.77±1.98 | 24.13±5.68 | 2.84±0.10 | 3.22±0.09 | 0.66 | 1.23 | 122 |
| | 80-92 | 6.3 | 140.62±2.46 | 14.29±7.12 | 2.24±0.10 | 2.77±0.09 | 0.63 | 1.13 | 122 |
| | 0-5 | 352.0 | 159.99±1.19 | 24.00±2.17 | 9.22±0.31 | 7.13±0.19 | 0.79 | 0.30 | 71 |
| STAR at | 5-10 | 299.0 | 160.58±1.16 | 24.97±2.17 | 8.34±0.28 | 6.75±0.18 | 0.78 | 0.27 | 71 |
| $\sqrt{s_{NN}} = 200$ GeV | 10-20 | 234.0 | 161.20±1.14 | 22.91±2.15 | 7.45±0.24 | 6.17±0.16 | 0.77 | 0.22 | 73 |
| | 20-30 | 166.0 | 162.27±1.12 | 23.05±2.17 | 6.31±0.20 | 5.60±0.14 | 0.75 | 0.25 | 75 |
| | 30-40 | 115.0 | 161.97±1.08 | 20.43±2.17 | 5.38±0.17 | 5.15±0.12 | 0.72 | 0.19 | 75 |
| | 40-50 | 76.0 | 162.97±1.08 | 21.01±2.21 | 4.46±0.14 | 4.64±0.11 | 0.69 | 0.13 | 75 |
| | 50-60 | 47.0 | 163.41±1.07 | 18.75±2.25 | 3.67±0.12 | 4.13±0.10 | 0.66 | 0.13 | 75 |
| | 60-70 | 27.0 | 162.39±1.06 | 16.47±2.31 | 2.95±0.10 | 3.79±0.09 | 0.61 | 0.26 | 75 |
| | 70-80 | 14.0 | 163.70±1.15 | 15.84±2.50 | 2.22±0.09 | 3.16±0.08 | 0.57 | 0.61 | 75 |
| | 0-10 | 328.0 | 150.60±1.39 | 23.07±3.51 | 9.26±0.25 | 8.65±0.21 | 0.73 | 0.43 | 114 |
| BRAHMS at | 10-20 | 239.0 | 151.38±1.48 | 26.53±3.72 | 8.07±0.23 | 7.68±0.19 | 0.72 | 0.42 | 114 |
| $\sqrt{s_{NN}} = 200$ GeV | 20-40 | 140.0 | 149.43±1.54 | 25.92±3.98 | 7.00±0.21 | 6.73±0.17 | 0.72 | 0.26 | 112 |
| | 40-60 | 62.0 | 148.36±2.02 | 26.69±5.21 | 5.02±0.20 | 5.38±0.17 | 0.68 | 0.52 | 112 |

laboration reports $\langle \delta y \rangle = 2.05$ for the 5% most central collisions at $\sqrt{s_{NN}} = 200$ GeV ($y_p = 5.36$) [26]. The results presented as the total charged-particle multiplicity per participating pair versus $N_{part}$ are gathered in Fig. 3. The predictions for PHENIX and STAR exhibit almost ideal centrality independence within the range of the PHOBOS measurement [24], i.e. $N_{part} \approx 60 - 360$. For BRAHMS and PHOBOS predictions some dependence can be observed but changes are within 10% over all the range. Also predicted values agree well with the data for both PHENIX cases, whereas for others agree within $\approx 10\%$.

Another simple test of the model can be performed with the use of the spectra of $\Omega$ hyperon. This is because $\Omega$ has only the thermal contribution to the invariant distribution, Eq. (2). Results together with the STAR data for $\Omega^- + \bar{\Omega}^+$ production at $\sqrt{s_{NN}} = 200$ GeV are presented in Fig. 4. Values of parameters for $20 - 40\%$ and $40 - 60\%$ centrality bins explored by STAR in $\Omega$ measurements are the averages of the values from Table I for bins which added percent coverage equals $20 - 40\%$ and $40-60\%$, respectively. One can see that predictions based on fits to PHENIX spectra agree well with the data. Predictions based on fits to STAR spectra agree only qualitatively, they have higher normalization. Also for the $0-5\%$ bin the slope differs. Blast-wave model based predictions for $\Omega^- + \bar{\Omega}^+$ spectrum for the $0 - 5\%$ bin of the preliminary STAR data were done in Ref. [10], but they

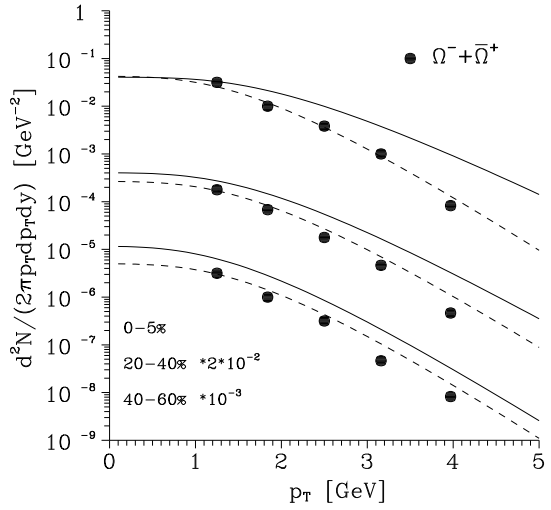


FIG. 4: Transverse momentum distributions of $\Omega^- + \bar{\Omega}^+$ for $\mid y \mid < 0.75$ in Au-Au collisions at $\sqrt{s_{NN}} = 200$ GeV. Data are from [27] (STAR) scaled for clarity, (statistical) errors are of the size of symbols. Lines denote model predictions: solid based on fits to the STAR spectra, dashed based on fits to the PHENIX spectra.

do not agree with the data neither in normalization nor in a slope. The probable reason for the worse agreement of the STAR data based predictions in the present model, Fig. 4, is that STAR spectra of identified stable hadrons are measured in narrower ranges of $p_T$ than PHENIX ones, i.e. $p_T \in [0, 1]$ GeV/c approximately for STAR [9] whereas for PHENIX $p_T \in [0.25, 2.95]$ GeV/c (pions), $p_T \in [0.55, 1.95]$ GeV/c (kaons) and $p_T \in [0.65, 4.25]$ GeV/c [(anti)protons] [23]. Also they differ in common ranges of $p_T$, namely STAR spectra are placed slightly above the corresponding PHENIX spectra and in the case of pions have different slopes (it has been checked carefully for the common $0-5\%$ bin after conversion of STAR spectra from $m_T - m_i$ to $p_T$). However, the STAR measurement of $\Omega^- + \bar{\Omega}^+$ is done within the range $p_T \in [1, 4]$ GeV/c, practically outside the STAR range of $p_T$ of identified stable hadrons but covering in great part PHENIX $p_T$ ranges.

In summary, the competitive hydrodynamical model has been proposed to describe hadronic $p_T$ spectra measured at relativistic heavy-ion collisions. So far, conclusions about chemical and thermal (kinetic) freeze-outs have been drawn from the blast-wave parametrization of the final stage of the collision [18]. It has turned out that those conclusions are not definite and depend strongly on the applied model. In the present model the temperature and the baryon number chemical potential at the kinetic freeze-out are almost independent of the centrality of the collision and their values are very close to the values at the chemical freeze-out, what is opposite to the conclusions drawn from the blast-wave model analysis [2].


[1] U. Heinz, Nucl. Phys. A **661**, 140 (1999).
[2] U. Heinz and G. Kestin, arXiv:nucl-th/0612105.
[3] G. Torrieri and J. Rafelski, J. Phys. Conf. Ser. **5**, 246 (2005) [arXiv:hep-ph/0409160].
[4] M. Kaneta and N. Xu, "Centrality dependence of chemical freeze-out in Au + Au collisions at RHIC", presented at QM2004 (Oakland) (only at arXiv:nucl-th/0405068).
[5] W. Florkowski, W. Broniowski and M. Michalec, Acta Phys. Polon. B **33**, 761 (2002).
[6] J. Cleymans, B. Kampfer, M. Kaneta, S. Wheaton and N. Xu, Phys. Rev. C **71**, 054901 (2005).
[7] P. Braun-Munzinger, D. Magestro, K. Redlich and J. Stachel, Phys. Lett. B **518**, 41 (2001).
[8] J. Rafelski, J. Letessier and G. Torrieri, Phys. Rev. C **72**, 024905 (2005).
[9] J. Adams *et al.* [STAR Collaboration], Phys. Rev. Lett. **92**, 112301 (2004).
[10] O. Y. Barannikova [STAR Collaboration], "Probing collision dynamics at RHIC", presented at QM2004 (Oakland) (only at arXiv:nucl-ex/0403014).
[11] O. Barannikova [STAR Collaboration], J. Phys. G **31**, S93 (2005).
[12] A. Baran, W. Broniowski and W. Florkowski, Acta Phys. Polon. B **35**, 779 (2004).
[13] P. Braun-Munzinger, K. Redlich and J. Stachel, in *Quark-Gluon Plasma 3*, eds R. C. Hwa and Xin-Nian Wang (World Scientific Publishing, Singapore, 2004), p. 491.
[14] K. Adcox *et al.* [PHENIX Collaboration], Phys. Rev. C **69**, 024904 (2004).
[15] J. M. Burward-Hoy [PHENIX Collaboration], Nucl. Phys. A **715**, 498 (2003).
[16] I. Arsene *et al.* [BRAHMS Collaboration], Phys. Rev. C **72**, 014908 (2005).
[17] B. B. Back *et al.* [PHOBOS Collaboration], arXiv:nucl-ex/0610001.
[18] E. Schnedermann, J. Sollfrank and U. Heinz, Phys. Rev. C **48**, 2462 (1993).
[19] W. Broniowski and W. Florkowski, Phys. Rev. Lett. **87**, 272302 (2001).
[20] W. Broniowski and W. Florkowski, Phys. Rev. C **65**, 064905 (2002).
[21] K. Hagiwara *et al.* [Particle Data Group Collaboration], Phys. Rev. D **66**, 010001 (2002).
[22] D. Prorok, Eur. Phys. J. A **24**, 93 (2005).
[23] S. S. Adler *et al.* [PHENIX Collaboration], Phys. Rev. C **69**, 034909 (2004).
[24] B. B. Back *et al.* [PHOBOS Collaboration], Phys. Rev. C **74**, 021902(R) (2006).
[25] D. Prorok, Phys. Rev. C **73**, 064901 (2006).
[26] I. G. Bearden *et al.* [BRAHMS Collaboration], Phys. Rev. Lett. **93**, 102301 (2004).
[27] J. Adams *et al.* [STAR Collaboration], Phys. Rev. Lett. **98**, 062301 (2007).